Author's Accepted Manuscript

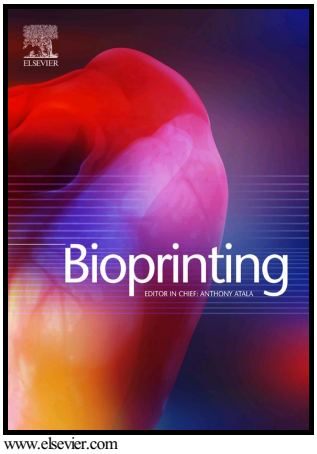

www.elsevier.com

3D Bioprinting of Liver-mimetic Construct with Alginate/Cellulose Nanocrystal Hybrid Bioink

Yun Wu, Zhi Yuan (William) Lin, Andrew C. Wenger, Kam C. Tam, Xiaowu (Shirley) Tang

PII: S2405-8866(17)30017-9
DOI: https://doi.org/10.1016/j.bprint.2017.12.001
Reference: BPRINT18

To appear in: *Bioprinting*

Received date: 25 August 2017
Revised date: 7 November 2017
Accepted date: 4 December 2017

Cite this article as: Yun Wu, Zhi Yuan (William) Lin, Andrew C. Wenger, Kam C. Tam and Xiaowu (Shirley) Tang, 3D Bioprinting of Liver-mimetic Construct with Alginate/Cellulose Nanocrystal Hybrid Bioink, *Bioprinting,* https://doi.org/10.1016/j.bprint.2017.12.001

3D Bioprinting of Liver-mimetic Construct with Alginate/Cellulose Nanocrystal Hybrid Bioink

*Yun Wu[1], Zhi Yuan (William) Lin[2], Andrew C. Wenger[1], Kam C. Tam[3], Xiaowu (Shirley) Tang[1,]**

[1]Department of Chemistry & Waterloo Institute for Nanotechnology, University of Waterloo, Canada, N2L 3G1.

[2]Ourotech, Inc., Waterloo, Ontario, Canada.

[3]Department of Chemical Engineering & Waterloo Institute for Nanotechnology, University of Waterloo, Canada, N2L 3G1.

***Corresponding Author**: X. S. Tang, Department of Chemistry & Waterloo Institute for Nanotechnology, University of Waterloo, 200 University Ave West, Waterloo, Ontario, Canada N2L 3G1, Email: tangxw@uwaterloo.ca. Phone: 1-519-888-4567 ext 38037, Fax: 1-519-746-0435

Abstract

3D bioprinting is a novel platform for engineering complex, three-dimensional (3D) tissues that mimic real ones. The development of hybrid bioinks is a viable strategy that integrates the desirable properties of the constituents. In this work, we present a hybrid bioink composed of alginate and cellulose

nanocrystals (CNCs) and explore its suitability for extrusion-based bioprinting. This bioink possesses excellent shear-thinning property, can be easily extruded through the nozzle, and provides good initial shape fidelity. It has been demonstrated that the viscosities during extrusion were at least two orders of magnitude lower than those at small shear rates, enabling the bioinks to be extruded through the nozzle (100 μm inner diameter) readily without clogging. This bioink was then used to print a liver-mimetic honeycomb 3D structure containing fibroblast and hepatoma cells. The structures were crosslinked with $CaCl_2$ and incubated and cultured for 3 days. It was found that the bioprinting process resulted in minimal cell damage making the alginate/CNC hybrid bioink an attractive bioprinting material.

Graphical abstract

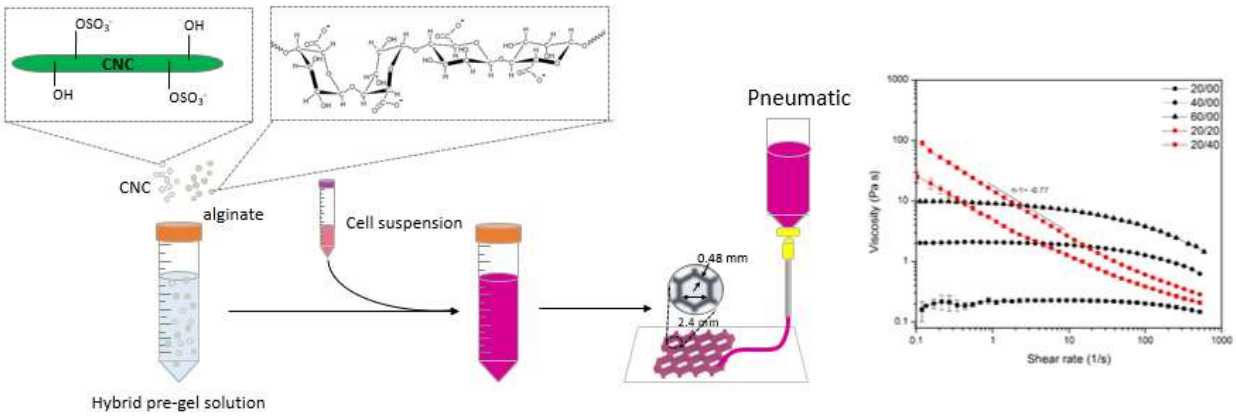

Keywords

Bioprinting, alginate, cellulose nanocrystals, tissue engineering, liver-mimetic structure

Introduction:

3D printing, otherwise known as additive manufacturing, is a term used to describe the process of fabricating a three-dimensional (3D) object layer by layer.[1,2] 3D bioprinting is a subset of 3D printing, which dispenses bioinks to construct complex 3D tissue architecture.[3] It allows for recapitulations of cell-

cell and cell-extracellular matrix (ECM) interactions that are absent in conventional two-dimensional (2D) *in vitro* cell culture but are crucial in modulating cellular behavior found under *in vivo* conditions. [4] The most commonly used bioprinting techniques are extrusion-based, particle fusion-based, light-induced, and inkjet-based bioprinting.[1–3,5–9] Extrusion-based bioprinting is one of the most popular techniques due to compatibility with a variety of bioink, ease of operation and relatively low cost. [3,10] Among various bioinks, hydrogels represent a class of promising materials because they provide a highly hydrated, biocompatible, 3D environment.[11–13]

Generally, a bioink should satisfy three requirements for extrusion-based bioprinting. First, the bioink should possess shear-thinning property, which ensures facile extrusion through a pressurized nozzle and good initial shape fidelity after extrusion.[13–17] Second, the bioink should have sufficient mechanical strength to support the bioprinted structure and retain its shape.[7] Third, the bioink should protect the encapsulated cells from mechanical stress during printing.[18]

Alginate is a natural polymer that has been extensively studied as a hydrogel material for tissue engineering applications due to its favorable properties, such as biocompatibility and easy processability.[19–21] Upon exposure to divalent cations such as Ca^{2+}, alginate undergoes a rapid and robust gelation process where the polymer chains form an "egg-box structure" with the divalent ions. [22,23] However, the rheological properties of pure alginate result in poor printability and pattern fidelity, which greatly limits its use in 3D bioprinting. [14,24]

Cellulose nanocrystals (CNCs) are rod-like or whisker-shaped nanoparticles extracted from the crystalline regions of cellulose fibers. In recent decades, its numerous favorable properties (e.g. renewability, low density, high mechanical strength, large and highly reactive surfaces, and low cytotoxicity) have attracted a significant amount of research interests for a variety of applications, including tissue engineering.[25–29] CNC can be mixed into various polymer matrices to reinforce the mechanical strength and induce shear thinning behavior.[28,30,31] For example, Siqueira et al. developed a hybrid ink comprising of CNC, 2-hydroxyethyl methacrylate (HEMA) monomer and polyether urethane acrylate (PUA). They found that the CNC particles align along the printing direction by shear flow, and

the CNC inks display shear-thinning behavior.[32] Hence, CNC is a suitable additive for enhancing the shear-thinning property of bioink.

In this work, we prepared a hybrid bioink by blending alginate and CNC, which combines the desirable properties and overcomes the inherent disadvantages of the individual components. Rheological properties such as shear-thinning, extrudability, and shape fidelity were investigated. An optimized bioink formulation was then selected to print a liver-mimetic 3D honeycomb structure, which was cultured with fibroblasts and hepatoma cells. It has been demonstrated that viability of cells encapsulated in this bioink is unaffected during printing.

Materials and Methods

Materials

Pharmaceutical grade sodium alginate (PROTANAL LF 10/60 FT) containing 60-70% G residues was acquired from FMC (Philadelphia, PA). CNC hydrolyzed from wood was supplied by Celluforce Inc. Phosphate-buffered saline was purchased from EMD Chemicals (Darmstadt, Germany). Calcium chloride was purchased from Sigma-Aldrich (St. Louis, Missouri). NIH/3T3 Fibroblast and human hepatoma cells, Eagle's Minimum Essential Medium (EMEM) and penicillin/ streptomycin were purchased from ATCC (Manassas, VA). Dulbecco's Modified Eagle's Medium (DMEM) and trypsin/EDTA solution were obtained from Lonza (Walkersville, MD). Fetal bovine serum (FBS) and trypan blue stain (0.4%) were provided by Gibco (Carlsbad, CA). LIVE/DEAD viability/cytotoxicity kit was purchased from Life Technologies (Carlsbad, CA).

Bioink Preparation

Dry CNC powder was dispersed in Milli-Q water to prepare 2, 4, 6, and 8% (w/v) CNC solutions. Similarly, dry alginate powder was weighed and dissolved in Milli-Q water to prepare 4% (w/v) and 6% (w/v) alginate solutions. To prepare the alginate/CNC hybrid pre-gel solutions, equal volumes of CNC and alginate solutions were mixed. Seven formulations of bioinks with different ratios of alginate and

CNC as listed in Table 1 were prepared. The pre-gel solution was sterilized by autoclaving at 121 ℃ for 20 min for cell culture.

Rheological Properties of the Hybrid Bioinks

The rheological properties of the inks were analyzed using a Bohlin-CS Rheometer with a cup and bob geometry (C25, bob diameter of 25mm and gap width of 150 μm). All measurements were conducted at room temperature.

Determination of Shear-Thinning

Using a constant rate testing mode, the steady-state shear viscosities of pure alginate (20/00, 40/00, and 60/00), and hybrid bioinks (20/10, 20/20, 20/30, and 20/40) were conducted over a range of shear rate of 0.1-500 s^{-1}.

Determination of Shear Rate

Power-law index (n) was calculated by curve-fitting the viscosity vs. shear rate curves using the power-law model:

$$\eta = K\dot{\gamma}^{n-1} \quad (1)$$

where K is the consistency, η is the viscosity, and $\dot{\gamma}$ is the shear rate. The shear rate at the nozzle wall can be obtained from the equation:

$$\dot{\gamma}_w = \frac{4Q}{\pi r^3}\left(\frac{3}{4} + \frac{1}{4n}\right) \quad (2)$$

where Q is the volumetric flow rate (16 μL/s) and r is the nozzle radius (50 μm).

Determinations of elastic and viscous moduli

A strain sweep from 0.05% to 10% was performed at a frequency of 1 Hz to determine the linear viscoelastic region (LVR). Subsequently, an optimized LVR strain of 0.1% was chosen for the oscillation frequency measurements performed from 0.1 to 10 Hz. The frequency sweeps were then used to define the elastic modulus (G') and the viscous modulus (G'').

Printability of Hybrid Bioinks

A designed syringe holder was printed in polylactic acid (PLA) using the thermoplastic extruder on a FlashForge Creator Pro (FlashForge, China). The original thermoplastic extruder from the x-axis carriage was then removed and replaced with the custom-made syringe holder. The modified FlashForge Creator Pro's operation software was unaltered, except for manual settings such as nozzle diameter, filament diameter, and extrusion temperature. Liver mimetic honeycomb models (1.75 mm spacing, 0.48 mm wall thickness, and 1.2 mm wall height as shown in Figure 1) were designed using Solidworks software and saved as an STL file. This file was then converted to G-code using ReplicatorG. The bioink-loaded syringe was equipped with a 32-gauge disposable tip (EFD Nordson, USA) and was fitted onto the plastic syringe holder. Applied extruding pressure ranged from 5 to 25 psi to control the ink flow rate to match the moving speed of the nozzle at 25 mm s^{-1}. The bioinks were deposited in 16 layers.

Morphologies of Hydrogels

The structures of hydrogel samples (20/00 and 20/40) were characterized using a field emission scanning electron microscope (FE SEM, Zeiss Leo 1530). The samples were first prepared in a custom-made Teflon mold and immersed in a 1% (w/v) $CaCl_2$ bath. The crosslinked hydrogels were instantly frozen in liquid nitrogen and lyophilized before being cut into small pieces with a sharp blade. The samples were then deposited onto an aluminum holder which was placed in a sputter coater, coating samples with a thin layer of gold. The pore size was analysed using ImageJ software.

3D Bioprinting of Liver-mimetic Tissue Constructs

Cell Culture

Fibroblasts were cultured in complete DMEM supplemented with 10% FBS and 100 unit/mL penicillin, 100 µg/mL streptomycin. Human hepatoma cells were cultured in EMEM with 10% FBS and 100 unit/mL penicillin, 100 µg/mL streptomycin. Both cell lines were maintained in a 5% CO_2 incubator at 37 ℃.

Bioprinting

For the construction of liver-mimetic structures, the outer honeycomb structures were first printed using one syringe with fibroblast-containing bioinks (10^6 cells/mL) using the aforementioned printing protocol. The inner cavities with a diameter of 1.5 mm were then printed using another syringe with bioink containing human hepatoma cells (10^6 cells/mL). The printed constructs were gelated in 1% (w/v) $CaCl_2$ solution for 10 min and then washed with serum-free DMEM. Next, the constructs were cultured in complete DMEM supplemented with 5 mM $CaCl_2$ in an incubator. Molded constructs were made as control samples using an extrusion-free method. Briefly, 20/40 bioink containing fibroblasts or hepatoma cells was placed on a sterilized glass slide with two spacers (150 μm thickness) and covered with an ion permeable membrane to make a slab (26 mm×26 mm×0.15 mm), which was then immersed in 1% (w/v) $CaCl_2$ for 10 min and was cultured in the same condition as that of the honeycomb constructs.

Cell Viability Studies

Viability of naked cells was assessed on day 0 using trypan blue stain and a hemocytometer. A LIVE/DEAD viability/cytotoxicity kit was utilized to determine the cell viability within the molded and bioprinted constructs on days 0, 1, and 3. Calcein-AM/ethidium homodimer was diluted in serum-free DMEM with ratios of 1: 2000 and 1: 500, respectively. The samples were first washed with serum-free DMEM for 10 min and then incubated in the staining solution for 2 hours. Afterwards, the samples were washed with serum-free medium for another 10 min. A fluorescence microscope (Nikon Eclipse Ti-S) was used to image the live and dead cells within the constructs. Images from each sample were taken and analyzed using ImageJ software. Cell viability was calculated by dividing the number of live cells by the total numbers of cells in the constructs.

Statistical analysis

All data were presented as mean ± standard deviation. Differences between samples were determined from the independent t-test and were considered statistically significant when $p < 0.05$.

Results and Discussion

Fabrication of Molded and Bioprinted Constructs

The overview of the sample fabrication process is illustrated in Figure 1. In brief, fibroblast and human hepatoma cells were trypsinized and added to the bioink, and the cell-laden bioink was either extruded through a nozzle for bioprinting or molded into a slab. The printed constructs and molded slabs were then further gelated by crosslinking the alginate chains in a $CaCl_2$ bath, followed by culturing in a $CaCl_2$-supplemented medium. The CNC used is produced by Celluforce Inc. with lengths of 200-400 nm and diameters of 10-20 nm as shown in Figure 2A. The CNC is derived from sulfuric acid hydrolysis with abundant negatively charged sulfate groups on the surface.

Rheological Properties of Hybrid Bioinks

Determination of Shear-Thinning. Figure 2B and Figure S1A show the viscosity vs. shear rate curves for all bioink formulations. It was found that despite higher viscosity associated with higher concentration, the curves for pure alginate (20/00, 40/00, and 60/00) all appeared to be relatively flat, suggesting that pure alginate has minimal shear-thinning property and is not suitable for bioprinting. On the other hand, the curves for hybrid bioinks were steep, where the addition of CNC greatly enhances shear-thinning property. A possible reason for the shear-thinning behavior is that alginate and CNC molecules are entangled randomly at static state, but re-aligned when shear stress is applied, thus lowering the viscosity of bioink (Figure 2C). In addition, the flow curves of the 2% (w/v) alginate bioinks converged as shear rate increased, indicating the addition of CNC does not have much effect on the viscosity of hybrid bioink at high shear rates. Moreover, after cells were suspended in the bioink at a concentration of 10^6 cells/mL, no significant changes in viscosity during extrusion were observed (Figure S2).

Determination of Shear Rate

Table 2 shows the power law index (n) and the shear rate values for bioinks containing 2% (w/v) alginate. All of the hybrid bioinks had n values that were smaller than 1, further confirming that the addition of CNC enhances the shear-thinning property. The shear rate exerted on the hybrid bioinks was approximately 200-300 s^{-1}, where the viscosities were at least two orders of magnitude lower than those at small shear rates, enabling the bioink to be readily extruded through the nozzle (100 μm inner diameter) with no clogging.

Determinations of Elastic and Viscous Moduli

Frequency sweeps at 0.1% strain measuring the elastic modulus (G') and viscous modulus (G'') of different formulations are shown in Figure 2D and Figure S1B. For all pure alginate bioinks, G'' values were higher than G' values over the frequency range, indicating that they are liquid-like. Hence, pure alginate gives poor shape fidelity and is not suitable for 3D bioprinting. On the other hand, the G' values were higher than G'' values for all hybrid bioinks, suggesting that hybrid pre-gel solutions are solid-like and they can provide good shape fidelity after extrusion.

Printability of Hybrid Bioninks

To evaluate the printability of the hybrid bioinks (20/10, 20/20, 20/30, and 20/40), they, along with 20/00, were loaded to print a liver-mimetic 3D honeycomb structure (Figure 3). As concentration of CNC increased, the geometries of the printed structure became increasingly well-defined, with 20/40 exhibiting the highest printing accuracy. Thus, 20/40 was selected as the best candidate for bioprinting.

Morphological Characterizations

SEM was employed to visualize the detailed pore structure with the 20/00 and 20/40 hydrogels and investigate the effect of CNC on the microstructure of the hybrid gel. The SEM micrograph of the pure alginate hydrogel showed a porous structure with wide-ranging microsized pores (7-178 μm; Figure

4A). On the other hand, the incorporation of CNC in the alginate network resulted in a highly porous microstructure with more uniform pores being ~20 μm in size (Figure 4B). The smooth surface of the pore walls of the hybrid hydrogels indicated the absence of CNC aggregation, suggesting that the CNCs were homogeneously dispersed in the alginate-based hydrogels matrix.

Cell Viability Studies

A 3D liver-mimetic honeycomb structure was designed as shown in Figure 5A**.** Figure 5B shows an image of the 3D structure immediately after bioprinting. Green and purple food dyes were utilized to differentiate the fibroblast-laden bioink (green) from the human hepatoma cells-laden bioink (purple). The viabilities of naked (before mixing with bioink) fibroblast and hepatoma cells were 96.47% and 92.75%, respectively. On day 0, the cell viabilities of the molded constructs were 70.73% for fibroblast and 55.07% for hepatoma, which could be attributed to mechanical stress during mixing and possibly the cytotoxicity of $CaCl_2$. The cell viabilities of fibroblast and hepatoma cells in bioprinted constructs on day 0 were 71.00% and 67.06%, respectively. No significant differences in cell viability were observed between molded and bioprinted constructs, indicating that the bioprinting process resulted in no observable cell death and thus is cell-compatible. However, after 3 days, cell viabilities of fibroblast and hepatoma cells decreased to 58.91% and 49.51%, respectively (Figure 5C). The declining viability over time may arise from the lack of cell-binding sites in the hydrogel, which limit cell adhesion, viability and proliferation. To circumvent such issue, one potential solution is incorporating polymers containing cell-binding sites, such as gelatin, into the system. There is an ever-growing amount of evidence reported in research literature that gelatin is effective in promoting the cell attachment due to its RGD tripeptide sequences, which are the major integrin-binding domains present within extracellular matrix (ECM).[33,34] Our preliminary results (Figure S4) show that the incorporation of gelatin in the alginate-CNC hybrid bioink does not influence the viscosity and hence printability of the bioink. Figures 5D-E show the

fluorescence images of homogeneously distributed fibroblasts and human hepatoma cells in the bioprinted constructs.

Conclusions

In this work, we developed a hybrid bioink by blending alginate with CNC. This bioink displayed excellent shear-thinning property, extrudability, and shape fidelity after deposition. The 20/40 (2% alginate and 4% CNC) bioink formulation was selected to print a liver-mimetic honeycomb 3D structure containing fibroblast and heptatoma cells, and the bioprinting process was found to induce minimal cell death. Overall, the proposed bioink has good potential for 3D bioprinting.

Acknowledgements:

The authors would like to thank Dr. Michael Tam's and Dr. Juewen Liu's group for providing access to the rheometer and fluorescence microscope, respectively. Also, we would like to thank Dr. Zengqian Shi, Debbie Wu, Yibo Liu, and Jimmy Huang for providing information on materials characterization and instruments training. This work is supported by a discovery grant from the Natural /Science and Engineering Research Council (NSERC) of Canada to Dr. Tang.

References:

(1) Fedorovich, N. E.; Alblas, J.; Wijn, J. R. DE; Hennink, W. E.; Verbout, A. J.; Dhert, W. J. A. *Tissue Eng.* **2007**, *13* (8), 1905–1925.

(2) Gross, B. C.; Erkal, J. L.; Lockwood, S. Y.; Chen, C.; Spence, D. M. *Anal. Chem.* **2014**, *86* (7), 3240–3253.

(3) Murphy, S. V; Atala, A. *Nat. Biotechnol.* **2014**, *32* (8), 773–785.

(4) Melchels, F. P. W.; Domingos, M. A. N.; Klein, T. J.; Malda, J.; Bartolo, P. J.; Hutmacher, D. W. *Prog. Polym. Sci.* **2012**, *37* (8), 1079–1104.

(5) Guvendiren, M.; Molde, J.; Soares, R. M. D.; Kohn, J. *ACS Biomater. Sci. Eng.* **2016**, *2* (10), 1678–1683.

(6) Jang, J.; Yi, H.; Cho, D. *ACS Biomater. Sci. Eng.* **2016**, *2* (10), 1722–1731.

(7) Billiet, T.; Vandenhaute, M.; Schelfhout, J.; Vlierberghe, S. Van; Dubruel, P. *Biomaterials* **2012**, *33* (26), 6020–6041.

(8) Landers, R.; Pfister, A.; John, H. *J. Mater. Sci.* **2002**, *37* (15), 3107–3116.

(9) Wüst, S.; Müller, R.; Hofmann, S. *J. Funct. Biomater.* **2011**, *2* (3), 119–154.

(10) Li, H.; Tan, Y. J.; Leong, K. F.; Li, L. .

(11) Hoffman, A. S. *Adv. Drug Deliv. Rev.* **2012**, *64* (64), 18–23.

(12) Lee, K. Y.; Rowley, J. A.; Eiselt, P.; Moy, E. M.; Bouhadir, K. H.; Mooney, D. J. *Macromolecules* **2000**, *33* (1), 4291–4294.

(13) Malda, J.; Visser, J.; Melchels, F. P.; Jüngst, T.; Hennink, W. E.; Dhert, W. J. A.; Groll, J.; Hutmacher, D. W. *Adv. Mater.* **2013**, *25* (36), 5011–5028.

(14) Markstedt, . Mantas, A. Tournier, I. vila, M. . gg , D. Gatenholm, P. *Biomacromolecules* **2015**, *16* (5), 1489–1496.

(15) Robert, B.; Iii, A. B.; Shepherd, R. F.; Hanson, J. N.; Nuzzo, R. G.; Wiltzius, P.; Lewis, J. A. *Adv. Mater.* **2009**, *21* (23), 1–4.

(16) Kolesky, D. B.; Truby, R. L.; Gladman, A. S.; Busbee, T. A.; Homan, K. A.; Lewis, J. A. *Adv. Mater.* **2014**, *26* (19), 3124–3130.

(17) Shepherd, J. N. H.; Parker, S. T.; Shepherd, R. F.; Gillette, M. U.; Lewis, J. A.; Nuzzo, R. G. *Adv. Funct. Mater.* **2011**, *21* (1), 47–54.

(18) Tan, Y. J.; Tan, X.; Yee, W.; Shu, Y. &; Tor, B. **2016**.

(19) Yeo, M. G.; Lee, J. S.; Chun, W.; Kim, G. H. *Biomacromolecules* **2016**, *17* (4), 1365–1375.

(20) Lee, C.; Shin, J.; Lee, J. S.; Byun, E.; Ryu, J. H.; Um, S. H.; Kim, D. I.; Lee, H.; Cho, S. W. *Biomacromolecules* **2013**, *14* (6), 2004–2013.

(21) Armstrong, J. P. K.; Burke, M.; Carter, B. M.; Davis, S. A.; Perriman, A. W. *Adv. Healthc. Mater.* **2016**, *5* (14), 1724–1730.

(22) Chen, K. L.; Mylon, S. E.; Elimelech, M.; Pennsyl, V. *Langmuir* **2007**, *23* (11), 5920–5928.

(23) Kuo, C. K.; Ma, P. X. *Biomaterials* **2001**, *22* (6), 511–521.

(24) Barnes, H. A.; Hutton, J. F.; Walters, F. R. S. K. *An introduction to rheology*; Elsevier: The Nertherlands, 1989; Vol. 3.

(25) Domingues, R. M. A.; Gomes, M. E.; Reis, R. L. *Biomacromolecules* **2014**, *15* (7), 2327–2346.

(26) Habibi, Y.; Lucia, L. A.; Rojas, O. J. *Chem. Rev.* **2010**, *110* (6), 3479–3500.

(27) Huq, T.; Salmieri, S.; Khan, A.; Khan, R. A.; Le, C.; Riedl, B.; Fraschini, C.; Bouchard, J.; Uribe-calderon, J.; Kamal, M. R.; Lacroix, M. *Carbohydr. Polym.* **2012**, *90* (4), 1757–1763.

(28) Moon, R. J.; Martini, A.; Nairn, J.; Youngblood, J.; Martini, A.; Nairn, J. *Chem. Soc. Rev.* **2011**, *40* (7), 3941–3994.

(29) Yang, X.; Cranston, E. D. *Chem. Mater.* **2014**, *26* (20), 6016–6025.

(30) Ureña-Benavides, E. E.; Ao, G.; Davis, V. A.; Kitchens, C. L. *Macromolecules* **2011**, *44* (22), 8990–8998.

(31) Kyle, S.; Jessop, Z. M.; Al-Sabah, A.; Whitaker, I. S. *Adv. Healthc. Mater.* **2017**, 1700264.

(32) Siqueira, G.; Kokkinis, D.; Libanori, R.; Hausmann, M. K.; Gladman, A. S.; Neels, A.; Tingaut, P.; Zimmermann, T.; Lewis, J. A.; Studart, A. R. *Adv. Funct. Mater.* **2017**, *27* (12), 1604619.

(33) Grigore, A.; Sarker, B.; Fabry, B.; Boccaccini, A. R.; Detsch, R. *Tissue Eng. Part A* **2014**, *20* (15–16), 2140–2150.

(34) Yu, J.; Gu, Y.; Du, K. T.; Mihardja, S.; Sievers, R. E.; Lee, R. J. *Biomaterials* **2009**, *30*, 751–756.

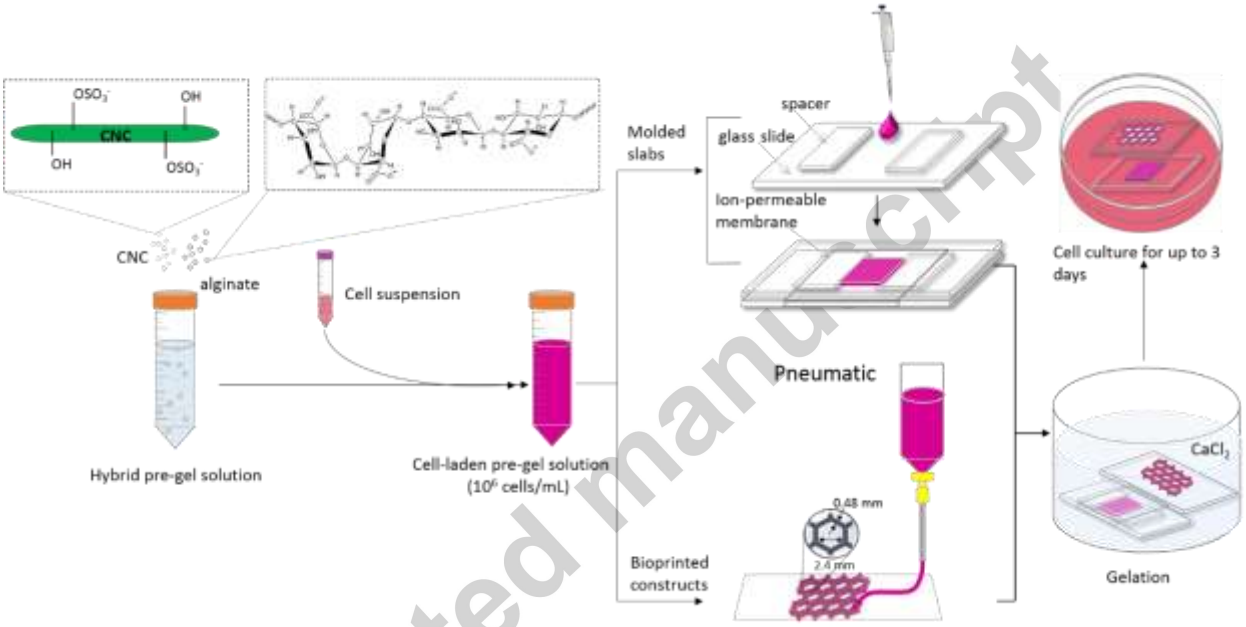

Figure 1. Schematic illustration of the fabrication process.

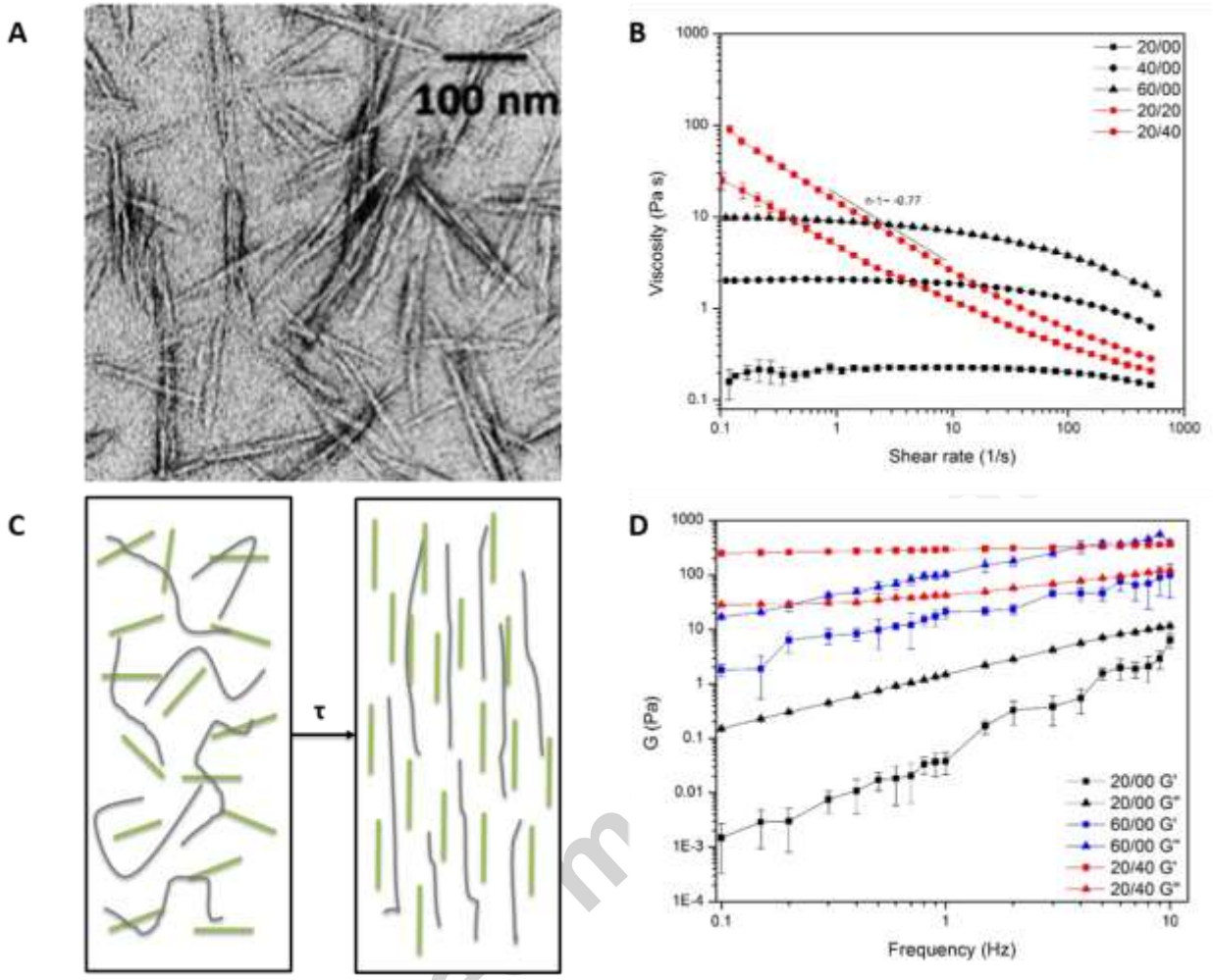

Figure 2. (A) TEM image of CNC used in this study. (B) Flow curves of five different bioink formulations, 20/00, 40/00, 60/00, 20/20, and 20/40. (C) Schematic illustration of interactions between alginate (grey) and CNC (green) at static state and under shear stress (τ). At static state (left), alginate and CNC are entangled in the hybrid solution randomly, while under shear stress (right), entangled alginate and CNC align. (D) Elastic modulus (G') and viscous modulus (G'') of three representative bioink formulations 20/00, 60/00, and 20/40 as a function of oscillatory frequency.

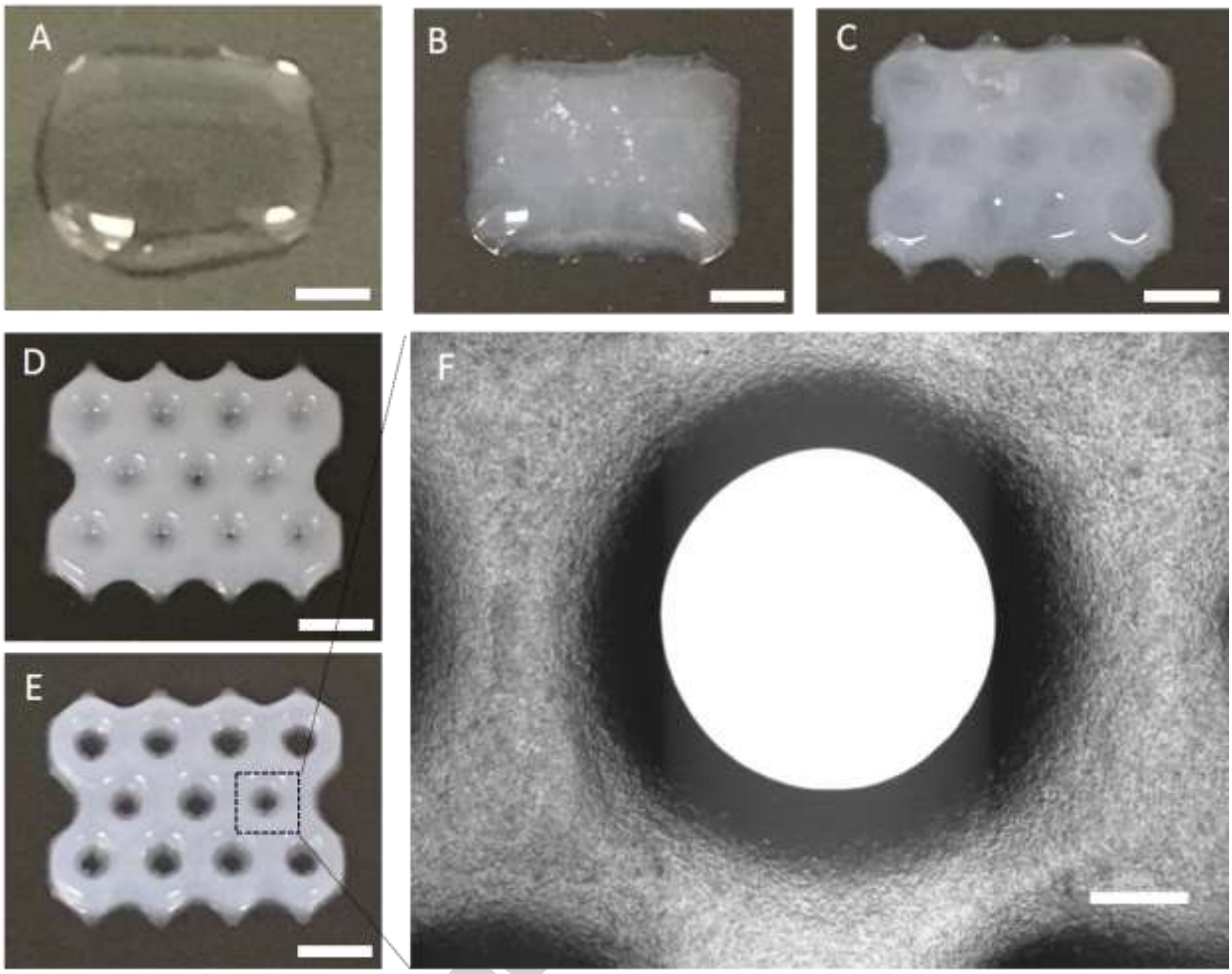

Figure 3. Optical images of 3D printed constructs using bioink formulations (A) 20/00, (B) 20/10, (C) 20/20, (D) 20/30, and (E) 20/40, respectively. (F) The zoomed-in image of the outlined area in (E). Scale bars are 5 mm in (A-E) and 500 μm in (F).

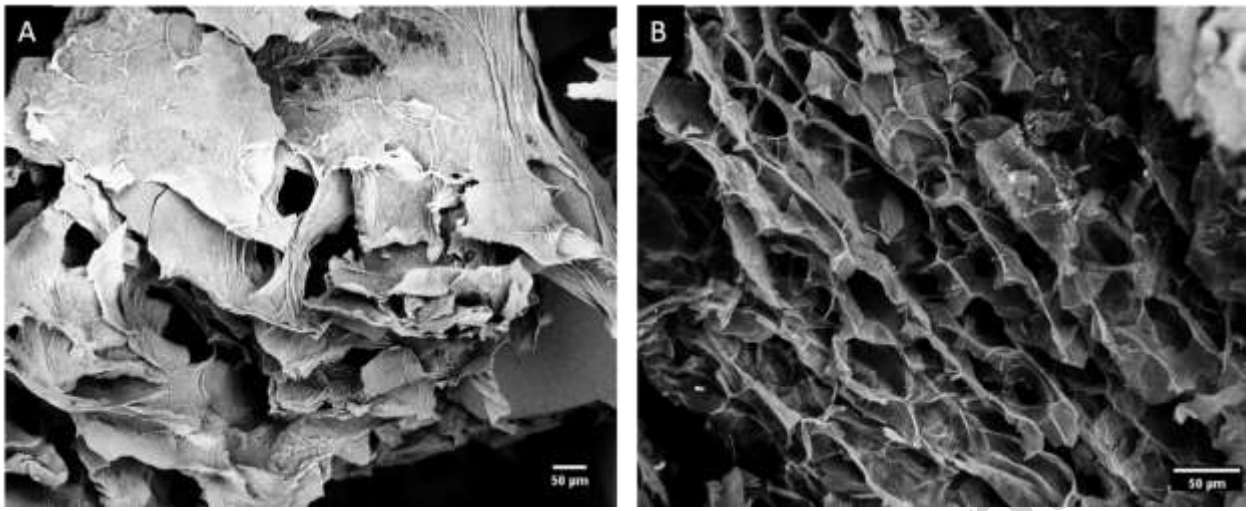

Figure 4. Scanning electron micrographs of freeze-dried (A) alginate (20/00) and (B) alginate/CNC (20/40) hydrogels.

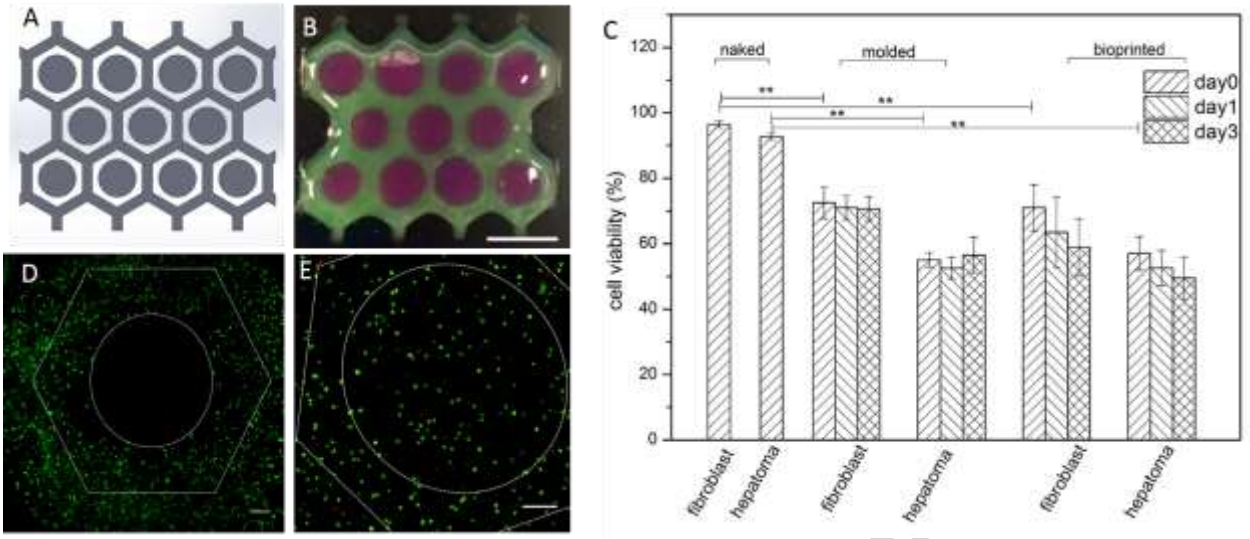

Figure 5. (A) Schematic top-down view of the liver-mimetic engineered tissue constructs. (B) 3D printed constructs with bioink 20/40. Food dyes were used to distinguish fibroblast-laden bioink (green) from hepatoma cell-laden bioink (purple). (C) Statistical analysis of viabilities (live cells populations/total cell populations) of fibroblast and human hepatoma cells on days 0, 1, and 3. (D&E) Representative live/dead fluorescent images of bioprinted (D) fibroblast only and (E) fibroblast plus human hepatoma cells. The dashed lines are the boundaries of the designed structure. The cells were stained with Calcein-AM and ethidium homodimer-1 to show live (green) and dead (red) cells. Scale bars are 5 mm in (B) and 250 μm in (D) and (E).

Table 1. Summary of bioink formulations.

Bioink formulation	Alginate (% w/v)	CNC (% w/v)	Water content (% w/v)
20/00	2	0	98
20/10	2	1	97
20/20	2	2	96
20/30	2	3	95
20/40	2	4	94
40/00	4	0	96
60/00	6	0	94

Table 2. Power-law index (n), shear rate ($\dot{\gamma}$), and viscosity (η) for bioinks containing 2% (w/v) alginate plus 0 %, 1 %, 2%, 3%, and 4% (w/v) CNC

Ink formula	n	$\dot{\gamma}_w$ (s^{-1})	η_w (Pa s)	τ_w (Pa)
20/00	0.697	180	0.245	44.1
20/10	0.559	195	0.345	67.3
20/20	0.271	272	0.266	72.4
20/30	0.247	287	0.341	97.9
20/40	0.225	303	0.551	166.9